Biochemistry

pubs.acs.org/biochemistry Article

DJ-1 Molecular Chaperone Activity Depresses Tau Aggregation Propensity through Interaction with Monomers

Daniela Jimenez-Harrison, Carol J. Huseby, Claire N. Hoffman, Steven Sher, Dalton Snyder, Brayden Seal, Chunhua Yuan, Hongjun Fu, Vicki Wysocki, Flaviano Giorgini, and Jeff Kuret*

Cite This: *Biochemistry* 2023, 62, 976–988 Read Online

ACCESS | Metrics & More | Article Recommendations

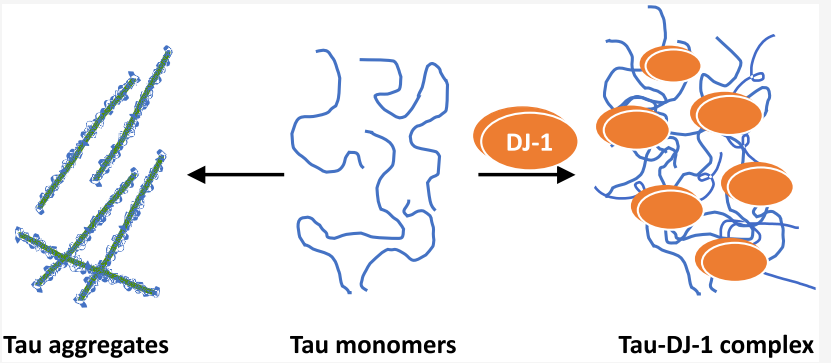

ABSTRACT: Tau aggregate-bearing lesions are pathological markers and potential mediators of tauopathic neurodegenerative diseases, including Alzheimer's disease. The molecular chaperone DJ-1 colocalizes with tau pathology in these disorders, but it has been unclear what functional link exists between them. In this study, we examined the consequences of tau/DJ-1 interaction as isolated proteins *in vitro*. When added to full-length 2N4R tau under aggregation-promoting conditions, DJ-1 inhibited both the rate and extent of filament formation in a concentration-dependent manner. Inhibitory activity was low affinity, did not require ATP, and was not affected by substituting oxidation incompetent missense mutation C106A for wild-type DJ-1. In contrast, missense mutations previously linked to familial Parkinson's disease and loss of α-synuclein chaperone activity, M26I and E64D, displayed diminished tau chaperone activity relative to wild-type DJ-1. Although DJ-1 directly bound the isolated microtubule-binding repeat region of tau protein, exposure of preformed tau seeds to DJ-1 did not diminish seeding activity in a biosensor cell model. These data reveal DJ-1 to be a holdase chaperone capable of engaging tau as a client in addition to α-synuclein. Our findings support a role for DJ-1 as part of an endogenous defense against the aggregation of these intrinsically disordered proteins.

INTRODUCTION

Tauopathies are a group of progressive neurodegenerative diseases associated with cognitive decline, with Alzheimer's disease (AD) being the most common form (reviewed[1]). They are defined pathologically by the appearance of lesions containing tau, an intracellular microtubule-associated protein that normally functions as an intrinsically disordered monomer but, in disease, converts into nonfunctional aggregated forms.[2,3] In model systems, aggregation follows nucleation–elongation kinetics,[4] characterized by the initial formation of an unstable nucleus, followed by energetically favorable aggregate extension through addition of monomers to the ends of growing polymers.[5,6] Mature tau aggregates have prion-like properties in biological model systems where they can "seed" misfolding and aggregation of normal tau monomers in naïve cell populations (reviewed[7]). Because tau aggregate formation can be toxic,[8] identification of proteostasis factors capable of resisting *de novo* nucleation or seeded conversion of tau into aggregates is a priority in the field.

Molecular chaperones constitute one of the cell's natural defenses against protein aggregation. They protect against inappropriate interactions (e.g., misfolding and aggregation) within crowded intracellular compartments through transient interactions with their client proteins.[9] The human molecular "chaperome" contains hundreds of members, including elements of the ATP-dependent Hsp70 and Hsp90 families and their associated co-chaperones.[10] Tau protein interacts

Received: October 11, 2022
Revised: January 19, 2023
Published: February 22, 2023

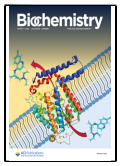

https://doi.org/10.1021/acs.biochem.2c00581
Biochemistry 2023, 62, 976–988

with members of these canonical families in model systems,[11] but the identities of pathophysiologically relevant chaperones have not been fully established.

Candidate tau chaperones are not limited to consensus members of the human chaperome. DJ-1, a primarily cytosolic 39-kDa homodimer encoded by the *PARK7* gene, is a noncanonical molecular chaperone structurally homologous to the DJ-1/PfpI/ThiJ protein superfamily, which includes bacterial chaperone Hsp31 and diverse enzymes possessing hydrolase or other enzymatic activities.[12−14] The former activity is mediated by surface residues acting independently of ATP hydrolysis[15] and is capable of modulating the aggregation and toxicity of proteins associated with neurodegeneration, including α-synuclein and huntingtin.[16,17] In contrast, the latter activity depends on a conserved catalytic triad involving a nucleophilic Cys residue.[12,13] Although human DJ-1 lacks a canonical catalytic triad[18] and expresses only weak hydrolase activity,[19,20] its Cys residue at position 106 remains highly reactive, with oxidation to sulfinic and sulfonic acid forms affecting DJ-1 subcellular localization and biological activity in model systems (reviewed[21]).

Consistent with a protective role for DJ-1 in neurodegenerative disease, certain *PARK7* mutations cause autosomal recessive forms of early-onset Parkinson's disease (PD) (reviewed[22]). One class of mutant, exemplified by M26I, perturbs DJ-1 folding by replacing residues buried in the hydrophobic core region.[23,24] A second class, exemplified by E64D, involves conservative substitution of surface residues but otherwise leaves DJ-1 folding unperturbed.[24] In cellular models, these mutants weaken the ability of DJ-1 to interact with clients such as α-synuclein, with M26I also weakening inhibition of α-synuclein oligomerization.[17]

Although DJ-1 is most closely linked with synucleinopathy, several lines of evidence indicate it may also interact with tau protein. First, DJ-1 colocalizes with tau lesions in Alzheimer's and other tauopathic neurodegenerative diseases,[25−27] suggesting a direct molecular interaction. Second, DJ-1 protein becomes oxidatively damaged in the brains of patients with AD as it does in idiopathic PD,[28] suggesting they share a common mechanism of DJ-1 activation. Finally, a DJ-1 mutation linked to familial PD (L172Q, a core region missense mutation) accumulates filamentous tau aggregates in addition to Lewy body pathology.[29] These data position DJ-1 as a candidate modulator of tau in addition to α-synuclein aggregation.

Tau and α-synuclein-bearing lesions frequently appear as copathologies in neurodegenerative diseases.[30] For example, tau pathology has been observed in both sporadic and familial forms of PD (reviewed[31]), whereas α-synuclein pathology is found in most AD cases, where it occasionally colocalizes with tau in the same cell.[32] Such neuropathological comorbidities correlate with worsening severity of clinical presentation and appear even in early-onset disease.[33,34] Commonalities in molecular chaperone interactions may contribute to the pathogenic synergy between tau and α-synuclein.

Here, we investigate the ability of human DJ-1 to chaperone 2N4R tau protein aggregation and seeding *in vitro*. In addition, we assess the chaperone activities of M26I and E64D as representative core and surface missense mutations, respectively, and C106A, an oxidation incompetent form of DJ-1. We show that DJ-1 can inhibit aggregation by acting on aggregation steps involving tau monomers, that its activity is not dependent on oxidation of C106, and that its tau chaperone activity can be compromised by disease-causing mutations. The results reveal that DJ-1 can chaperone tau protein under aggregation-promoting conditions.

EXPERIMENTAL PROCEDURES

Protein Preparation. Full-length human tau (2N4R isoform; UniProt Accession ID P10636-8) and its deletion mutant A2_P251del L376_L441del (Δ4R construct) were expressed in BL21CodonPlus (DE3)-RP *Escherichia coli* cells (Agilent) and purified, as described previously.[35] Human DJ-1 (UniProt Accession ID Q99497) encoded by plasmid DJ-1 TEV site pET15b was a gift from Mark Wilson (Addgene plasmid #60687; http://n2t.net/addgene:60687; RRID:Addgene_60687). This vector drives expression of DJ-1 fused to a poly-His sequence via a TEV-cleavable linker. DJ-1 missense mutants M26I, C106A, and E64D were created from DJ-1 pET15b by site-directed mutagenesis using the QuikChange Lightning Kit (Agilent). Recombinant DJ-1 fusion proteins were prepared from *E. coli* by French pressure cell lysis (10 000 psi) and immobilized metal affinity chromatography (IMAC). Poly-His tags were removed by diluting DJ-1 fusion proteins to 2 mg/mL in Lysis buffer (500 mM NaCl, 20 mM Tris, pH 8.0) containing phenylmethylsulfonyl fluoride (PMSF) and incubating overnight with TEV protease (prepared and used as described[36]) within dialysis tubing (32-mm diameter dialysis; VWR #25225-248). Cleaved poly-His tags and undigested DJ-1 fusion proteins were then removed from the preparations by IMAC, whereas DJ-1 proteins were collected from flow-through fractions concentrated by centrifugal ultrafiltration (10k molecular weight cutoff; Millipore #UFC901024) and polished by size exclusion chromatography (Sephacryl S-100 operated in 10 mM HEPES-HCl, 100 mM NaCl, 0.1 mM EGTA, pH 7.4). Protein purity was ascertained by SDS-PAGE, and concentration was determined using the bicinchoninic acid (BCA) method.[37]

NMR Spectroscopy. Recombinant His-tagged Δ4R tau was labeled in M9 minimal medium containing ^{15}N-NH_4Cl as described previously[38] and then purified as described above and thrombin-treated (1 U/mg tau, 4 °C overnight) to yield nontagged ^{15}N-Δ4R tau. For NMR binding studies, samples contained 50 μM ^{15}N-labeled Δ4R Tau in NMR buffer (50 mM sodium phosphate pH 6.8, 10 mM NaCl, 10% (v/v) D_2O) and, when present, unlabeled DJ-1 (1:1 stoichiometry). After a 2 h incubation at room temperature, two-dimensional ^{1}H−^{15}N heteronuclear single quantum coherence (HSQC) spectra were acquired (300 K) on a Bruker Advance III HD 800 MHz spectrometer equipped with a 5 mm triple-resonance inverse cryoprobe and Z-Gradients. Spectra were acquired using 16 scans per increment with spectral widths of 12 820 and 2270 Hz in the ^{1}H and ^{15}N dimensions, respectively. Data were processed and analyzed with TopSpin (Bruker Corp.) based on deposited assignments[39] for K18 tau (BioMagResBank accession number 19253). Signal intensity ratios (I/I_0) were calculated from these data as described previously.[11,40]

Mass Spectrometry. Proteins were buffer-exchanged twice sequentially into 100 mM ammonium acetate (pH 6.8) using Micro Bio-Spin P6 columns with a 6 kDa size cutoff and adjusted to 1 μM final concentration. Native mass spectrometry experiments were performed on a Thermo Scientific Q Exactive UHMR Hybrid Quadrupole-Orbitrap Mass Spectrometer previously modified with a surface-induced dissociation cell replacing the transfer multipole prior to the C-trap.[41] Proteins were transferred from the solution to the gas phase by nanoelectrospray ionization (nESI) from in-house pulled

https://doi.org/10.1021/acs.biochem.2c00581
Biochemistry 2023, 62, 976−988

borosilicate capillaries (via a Sutter Instruments P-97 micropipette tip puller, Novato, CA). Approximately 5 μL of the sample was loaded into the nESI emitter, and ∼1 kV was applied to the solution to generate ions. Mass spectra were acquired as an average of ∼60 scans using the following settings: resolution, 12k; trap gas, 4; in-source trapping, up to 60 V to desolvate complexes for accurate mass measurements; capillary temperature, 250 °C. Deconvolution of charge state distributions was performed with Unidec.[42] Predicted average masses were calculated from the expected sequences using ProtParam (https://web.expasy.org/protparam/).

Tau Aggregation. To aggregate tau monomers, recombinant human 2N4R tau preparations (1.5 μM) were incubated (24 h at 37 °C without agitation) in Assembly Buffer (10 mM HEPES, 100 mM NaCl pH 7.4, 5 mM dithiothreitol) in the presence or absence of DJ-1 proteins (0−4.5 μM) and aggregation inducers Geranine G (100 μM, TCI America[43]) or octadecyl sulfate (ODS, 50 μM, Lancaster[44]). Aggregation products were then analyzed by TEM, laser light scattering, or sedimentation assays described below.

To disaggregate tau, 2N4R tau filaments prepared as described above in the absence of DJ-1 were divided into two separate microfuge tubes, diluted 6% by the addition of either water or DJ-1 (4.5 μM final DJ-1 concentration), and then incubated at 37 °C without agitation. Aliquots were removed from each sample after 0, 2, 4, and 6 h incubation and subjected to TEM assay as described below.

Laser Light Scattering. Aggregate reactions (120 μL) were transferred to quartz cuvettes (3 × 3 mm) and illuminated with a diode-pumped solid-state laser (λ = 635 nm; Optotronics). Scattered light was captured at an angle of 90° to the incident lighting using a CMOS digital camera (DMK 22BUC03; Imaging Source) operated at an aperture of *f*/22 and an exposure time of 35 ms. Captured images were imported into ImageJ software,[45,46] and the intensity of scattered light (I_s (90°)) was estimated from the average value of a 10 × 10 pixel region of interest. The scattering intensity captured at zero exposure time (dark current) was subtracted from all measurements as described previously.[47] Measurements were collected from biological replicates (n = 3).

Transmission Electron Microscopy (TEM). Aliquots of aggregation reactions (50 μL) were adsorbed onto 300-mesh formvar/carbon-coated grids (Electron Microscopy Services), stained with 2% (w/v) uranyl acetate, and imaged on the FEI Tecnai G2 Spirit TEM as described previously.[43] At least three images were captured at random from each experimental condition at 15−35k-fold magnification using a MacroFire camera (Optronics). Aggregate lengths were measured and calibrated with scale bars using ImageJ. Total fibril length per grid was calculated as the sum of the lengths of all fibrils in a single image. Measurements were collected from technical replicates (n = 4−6 images).

Sedimentation. Aggregate reactions (100 μL) were centrifuged (100 000*g* for 1 h at 4 °C). The resulting supernatant fraction was carefully removed, whereas the pellet was resuspended in an equal volume of Assembly Buffer. All samples were then boiled for 5 min in SDS sample buffer, and then equal volumes of supernatant and pellet samples were subjected to SDS-PAGE (4−20% acrylamide; BioRad TGX) with Coomassie Blue staining (Precision Plus Protein Standards, BioRad). The resulting proportion of soluble tau in the supernatant versus insoluble tau in the pellet was quantified by densitometry using the ImageJ gel analyzer tool.[45] Band densities were normalized as a fraction of the sum of the supernatant and pellet for each reaction. Measurements were made from biological replicates (n = 3).

Cell Seeding Assays. DS9 seeds were prepared from DS9 HEK293 cells.[48] After cell breakage in PBS containing 0.05% Triton X-100 and 1 x Halt protease/phosphatase inhibitor cocktail (Thermo #78440), lysates were centrifuged sequentially at 500*g* (5 min) and 1000*g* (5 min) at 4 °C and then divided into 5−10 μL aliquots. Synthetic 2N4R tau seeds were obtained from aggregates prepared, as described above. These were centrifuged at 100 000*g* for 1 h to yield a pellet fraction that was resuspended in Assembly Buffer and then divided into aliquots without additional shearing or sonication. Both DS9 and 2N4R tau preparations were quantified for protein content by BCA assay and then stored at −80 °C for one-time use.

Seeding activity was quantified in biosensor cells (Tau RD P301S FRET Biosensor; ATCC CRL-3275)[49] maintained in Dulbecco's modified Eagle's medium supplemented with 10% FBS, 1% penicillin−streptomycin, and 2 mM L-alanyl-L-glutamine in a humidified atmosphere (37 °C and 5% CO_2). Cells were plated in 12-well plates at a density of 1 × 10^5 cells and grown for 24 h to 60% confluency. Tau seeds incubated with recombinant DJ-1, M26I, or control BSA for 16 h at 37 °C were transfected into these cells with Lipofectamine 3000 for 24 h.

Biosensor cell seeding was detected using flow cytometry (BD LSR Fortessa Cell Analyzer) as described previously.[49] In brief, cells were harvested with trypsin neutralized with media containing 10% FBS, washed, and resuspended in PBS containing 1% BSA. To detect CFP and FRET, cells were excited with 405 nm laser light and fluorescence-detected on 450/40 and 525/50 nm band-pass filters, respectively. FRET signals were quantified using the gating strategy described previously.[50] FRET positivity, defined as the percentage of cells gated in the FRET channel, was used for all analyses. Three biological replicates were performed per condition, with each replicate capturing 30 000−50 000 events. Data were analyzed and compensated using Kaluza analysis software version 2.1 (Beckman Coulter).

Data Analysis. Tau aggregation lag time, minimal concentration (K_{min}), and protomer dissociation rate constant (k_e^-) were estimated as described previously.[43] Briefly, aggregation lag times (defined as the time when the tangent to the point of maximum aggregation rate intersects the abscissa of the sigmoidal curve)[51] were obtained from time series by nonlinear regression with a three-parameter Gompertz growth function.[52] Minimal concentrations required to support aggregation were estimated by extrapolating the tau concentration dependence of total filament length to the abscissa intercept. Protomer dissociation rate constant (k_e^-) was obtained from the exponential decay of filament length as a function of time.

Inhibition of tau aggregation (y) as a function of DJ-1 concentration (x) was quantified with the hyperbola

$$y = \frac{y_{max} \times x}{IC_{50} + x} \quad (1)$$

where y_{max} represents the maximum inhibition at plateau and IC_{50} is the concentration of DJ-1 at half-maximal inhibition.

https://doi.org/10.1021/acs.biochem.2c00581
Biochemistry 2023, 62, 976−988

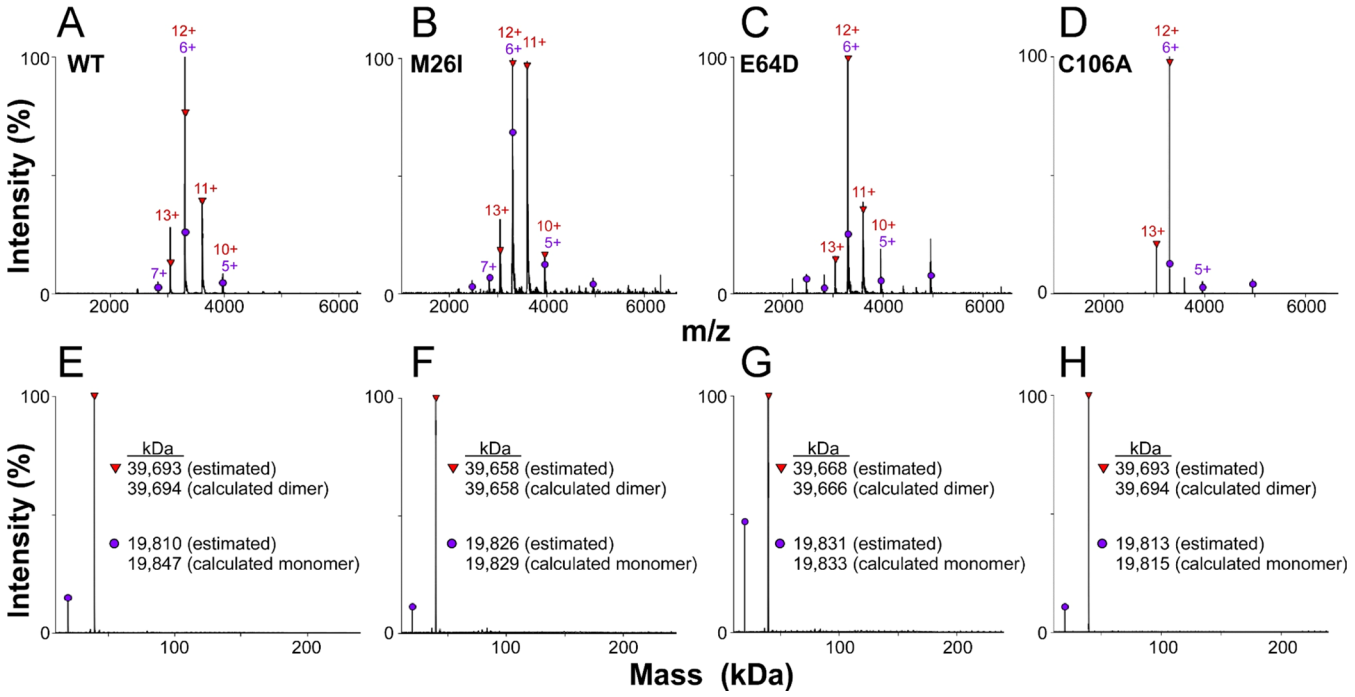

Figure 1. Recombinant DJ-1 is primarily a dimer in solution. (A–D) nMS charge state distributions in the 1000–6000 m/z range and (E–H) deconvolved masses for (A, E) wild-type DJ-1 (WT) and mutants (B, F) M26I, (C, G) E64D and (D, H) C106A, where red triangles and purple circles symbolize dimers and monomers, respectively. These data indicate that all recombinant DJ-1 preparations shared primarily a dimeric quaternary structure.

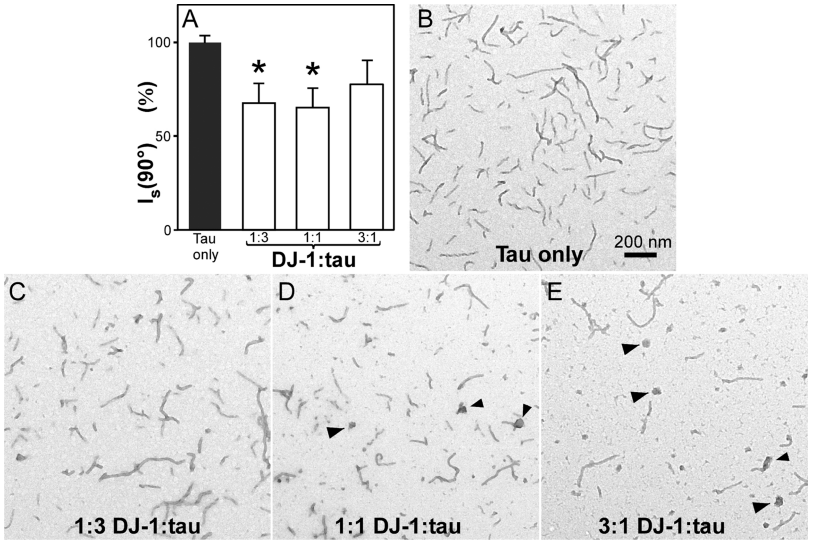

Figure 2. DJ-1 suppresses tau aggregation. 2N4R tau protein (1.5 μM) was incubated under aggregation conditions for 24 h in the absence and presence of purified recombinant DJ-1 and then assayed for fibrillation. (A) Laser light scattering assay, where each bar represents the normalized light scattering intensity (I_s (90°)) ± S.D. (n = 3). Light scattering intensity changed biphasically in the presence of DJ-1, reaching a minimum at 1:3 and 1:1 DJ-1:tau ratios (*p < 0.05 compared to the tau-only condition; ANOVA with Dunnett's *post-hoc* test). (B–E) Representative TEM assay, where each panel is a representative micrograph collected at the stated condition. (B) In the absence of DJ-1, tau aggregated to form filaments. (C–E) Although increasing DJ-1 concentrations depressed tau fibrillation monotonically, the highest DJ-1:tau ratios also generated large amorphous aggregates (arrowheads).

Biosensor cell FRET positivity data (y) as a function of seed protein amount (x) were fitted by the four-parameter logistic function

$$y = y_{\min} + \frac{y_{\max}}{1 + \left(\frac{x}{EC_{50}}\right)^{n}} \quad (2)$$

where $y_{\min}$ and $y_{\max}$ represent the minimum and plateau FRET positivity in the absence and presence of seeds, respectively, n is the Hill coefficient, and EC_{50} is the concentration of seeds at 50% of plateau FRET positivity.

All measured parameters are reported ± S.D., whereas those estimated through parametric fitting are reported ± standard error of the estimate (SEE). Differences among assay groups

https://doi.org/10.1021/acs.biochem.2c00581
Biochemistry 2023, 62, 976–988

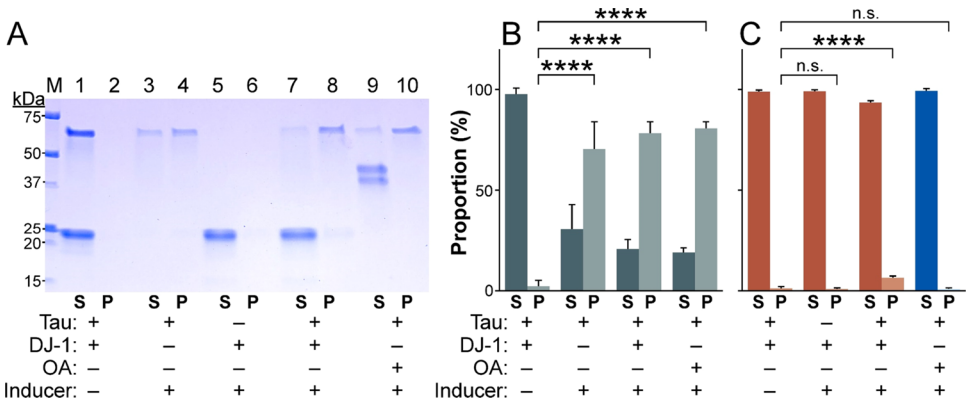

Figure 3. Sedimentation assay. (A) Representative SDS-PAGE of pellet (P) and supernatant (S) fractions from aggregation reactions performed in the absence (−) and presence (+) of 2N4R tau, DJ-1, or ovalbumin (OA) and Geranine G inducer. M, Marker proteins calibrated in kDa. (B) Proportion of 2N4R tau (green) and (C) either DJ-1 (red) or OA (blue) in pellet and supernatant fractions quantified by densitometric analysis after SDS-PAGE (n.s., not significant; ****$p < 0.0001$, ANOVA with Dunnett's *post-hoc* test).

were analyzed by one-way ANOVA and Dunnett's post-hoc multiple comparison test using GraphPad Prism software, whereas pairwise comparisons were analyzed by *t*-test. For all data, the null hypothesis was rejected at $p < 0.05$.

RESULTS

Recombinant DJ-1 Proteins are Dimers in Solution. Human DJ-1 and mutants M26I, E64D, and C106A were expressed as His-tagged fusion proteins in *E. coli*. After purification by immobilized metal affinity chromatography, His tags were removed using Tobacco Etch Virus (TEV) protease and gel filtration chromatography to yield preparations consisting of 189 amino acid subunits containing N-terminal Ser instead of Met. Because DJ-1 chaperone function depends in part on the maintenance of dimeric quaternary structure,[17] the composition of all recombinant DJ-1 preparations was interrogated using native mass spectrometry (nMS). Two charge state distributions were identified, ranging from 13+ to 10+ for the first and 7+ to 4+ for the second (Figure 1A−D).

Mass spectra deconvolution revealed that the first distribution contained major proteoforms corresponding to the predicted molecular weights for protein dimers (Figure 1E−H). In contrast, the second distribution corresponded to a minor component consisting of dissociated protein monomers (Figure 1E−H). The absolute levels of monomer in each preparation depend in part on the relative gas-phase stability of dimers and their sensitivity to the in-source collisional activation applied to all samples for accurate mass measurement. Nonetheless, the relative intensity of deconvolved nMS data reveal that the dominant oligomeric state of all recombinant DJ-1 and mutant preparations after heterologous expression and TEV cleavage is the dimer, with no evidence for higher molecular weight species.

DJ-1 Modulates Tau Aggregation *In Vitro*. To investigate the ability of DJ-1 to chaperone tau protein aggregation, recombinant full-length human 2N4R tau was incubated in the absence and presence of the DJ-1 preparations described above and aggregation inducer Geranine G. These conditions were employed because they support aggregation of tau at physiological low micromolar tau concentrations[53] under near-physiological conditions of pH, reducing conditions, and ionic strength.[5,54,55] Moreover, aggregation under these conditions approximates a homogeneous nucleation scheme characterized by the initial formation of an unstable dimeric nucleus followed by filament elongation through monomer addition.[5] As reported previously, 2N4R tau alone formed filamentous aggregates that were observable by transmission electron microscopy (TEM) and laser light scattering methods (Figure 2A,B). Introduction of DJ-1 at substoichiometric DJ-1 concentrations (i.e., 1:3 DJ-1:tau ratio) depressed both light scattering intensity (Figure 2A) and total filament lengths (Figure 2C). As DJ-1 rose to stoichiometric levels (i.e., 1:1 DJ-1:tau), the light scattering signal remained depressed (Figure 2A), whereas filament length observed by TEM decreased further and was accompanied by the appearance of globular co-aggregates (Figure 2D). At suprastoichiometric DJ-1 levels (3:1 DJ-1:tau), light scattering intensity rebounded toward control levels (Figure 2A), whereas filament lengths decreased still further, and the globular co-aggregates became more pronounced (Figure 2E).

These data show that DJ-1 can depress tau aggregation in a concentration-dependent manner. They also suggest that DJ-1 and tau form large nonfilamentous complexes that confound light scattering methods.

To test this hypothesis, products of aggregation reactions were separated into soluble and pellet fractions by ultracentrifugation and detected by SDS-PAGE (Figure 3A). In the absence of Geranine G inducer, both DJ-1 and 2N4R tau distributed almost exclusively into the soluble fraction (Figure 3B,C). However, incubation of tau alone with Geranine G shifted it primarily into the insoluble fraction (Figure 3B,C), consistent with its aggregation. In contrast, DJ-1 incubated alone with Geranine G remained soluble. These data confirm that Geranine G is an inducer of tau but not DJ-1 aggregation. Nonetheless, when DJ-1 and tau were incubated together (3:1 ratio) in the presence of Geranine G inducer, a significant portion of DJ-1 joined tau in the insoluble fraction (Figure 3B,C). This association did not appear to result from nonspecific trapping within tau aggregates because ovalbumin failed to partition into the pellet fraction when present as a replacement for DJ-1 (Figure 3C). Taken together, TEM, light scattering, and sedimentation data indicate that DJ-1 can antagonize tau filament formation at stoichiometric concentrations while yielding nonfilamentous complexes composed of tau and DJ-1. Because of its ability to resolve filamentous from amorphous morphology, the TEM assay was used for all subsequent experiments.

https://doi.org/10.1021/acs.biochem.2c00581
Biochemistry 2023, 62, 976−988

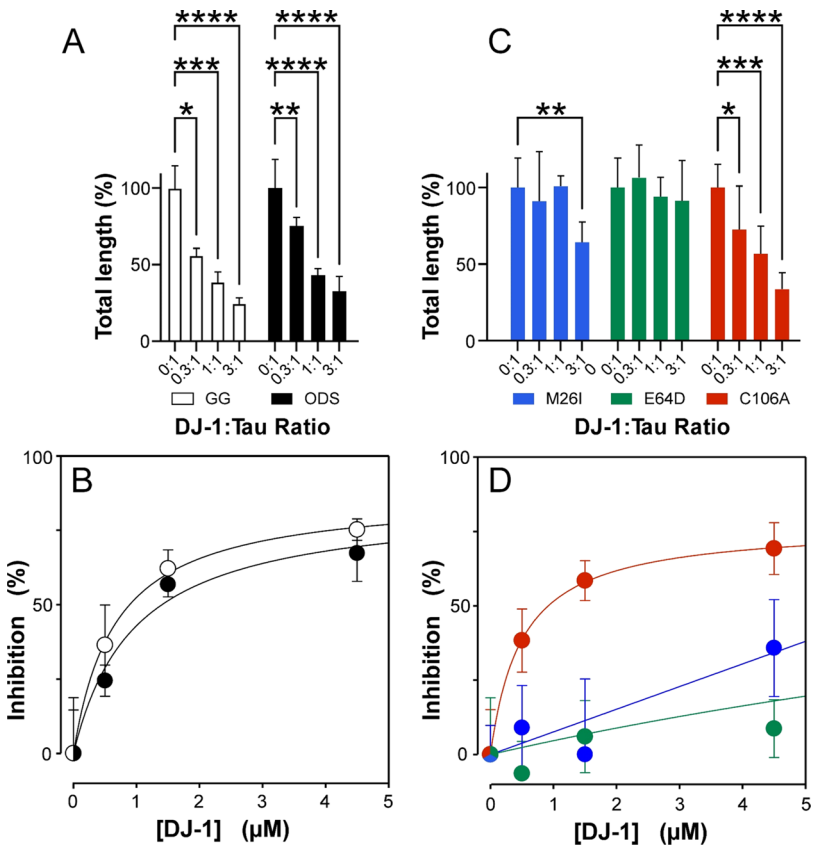

Figure 4. DJ-1 mutants vary with respect to tau chaperone activity. 2N4R tau protein (1.5 μM) was incubated under aggregation conditions for 24 h in the absence or presence of purified recombinant wild-type (WT) DJ-1 or mutants M26I, E64D, and C106A at varying molar ratios and then assayed for fibrillation using TEM. (A) WT DJ-1 tested with Geranine G (GG) and ODS inducers, where each bar represents aggregation as a normalized percentage of total filament length/field in the absence of DJ-1 ± S.D. (*$p < 0.05$; **$p < 0.01$; ***$p < 0.001$; ****$p < 0.0001$ compared to the tau-only condition; ANOVA with Dunnett's *post-hoc* test). (B) Replot of Panel (A) data, where data points represent the mean percent inhibition of aggregation relative to the tau-only condition ± S.D. and the solid lines represent the best fit of the data points to eq 1. (C) DJ-1 mutants M26I, E64D, and C106A tested with Geranine G inducer, with ANOVA performed as described in Panel (A). (D) Replot of Panel (C) data, with nonlinear regression performed as described for Panel (B).

Disease-Associated DJ-1 Mutations Differentially Affect Tau Chaperone Tau Activity. To quantify chaperone activity toward 2N4R tau, wild-type DJ-1, disease-associated mutants M26I and E64D, and oxidation incompetent mutant C106A were tested in the TEM assay. Wild-type DJ-1 significantly depressed total filament length at all tested concentrations in the range 0.5−4.5 μM (Figure 4A). The concentration dependence appeared saturable without evidence of cooperativity, indicating the absence of tight binding kinetics despite the analytes being present at stoichiometric concentrations.[56] Fitting these data with a one-site saturation binding isotherm yielded an estimate of affinity (IC_{50}) of 0.66 ± 0.06 μM with 87.2 ± 2.4% aggregation inhibition predicted at saturation (Figure 4B). These data show that DJ-1 is an effective 2N4R tau chaperone at stoichiometric DJ-1:tau ratios, but like members of the classical chaperome, its interaction is low affinity (reviewed[57]). To test whether chaperone activity was inducer-specific, an identical titration was performed with ODS, a tau aggregation inducer that functions in micellar form[44] (Figure 4A). Fitting the resulting data with a one-site saturation binding isotherm yielded an IC_{50} of 0.97 ± 0.35 μM with 84.4 ± 10.2% aggregation inhibition at saturation (Figure 4B). These data show that wild-type DJ-1 can antagonize 2N4R tau fibrillation driven by structurally diverse anionic inducers.

A similar inhibitory profile was observed for DJ-1 mutant C106A in the presence of Geranine G inducer (IC_{50} = 0.50 ± 0.02 μM; Figure 4A,B), indicating that oxidation of the DJ-1 redox sensor was not required for chaperone activity on tau protein. In contrast, mutant M26I was active only at the highest tested concentration, whereas E64D was inactive at all tested concentrations. These data indicate that two representative mutants associated with autosomal recessive PD have weakened chaperone activity against 2N4R tau protein.

DJ-1 Antagonizes Nucleation and Elongation Phases of Tau Aggregation. Chaperone proteins differentially interfere with nucleation and/or elongation steps of tau aggregation.[11] To characterize the mechanism of DJ-1 chaperone activity, the effects of wild-type DJ-1 on the time-dependent evolution of 2N4R total filament length were investigated using TEM. In both the presence and absence of stoichiometric concentrations of DJ-1, Geranine G-induced 2N4R tau fibrillation displayed sigmoidal kinetics comprising initial lag, exponential growth, and final plateau phases (Figure 5A). However, the presence of DJ-1 lengthened the lag phase nearly 2-fold, indicating a slowing of the rate-limiting step of nucleation-dependent aggregation (Figure 5B). DJ-1 also depressed total aggregate levels at the plateau, indicating a decrease in tau supersaturation (Figure 5A). Consistent with this observation, the minimal concentration of tau protein

https://doi.org/10.1021/acs.biochem.2c00581
Biochemistry 2023, 62, 976−988

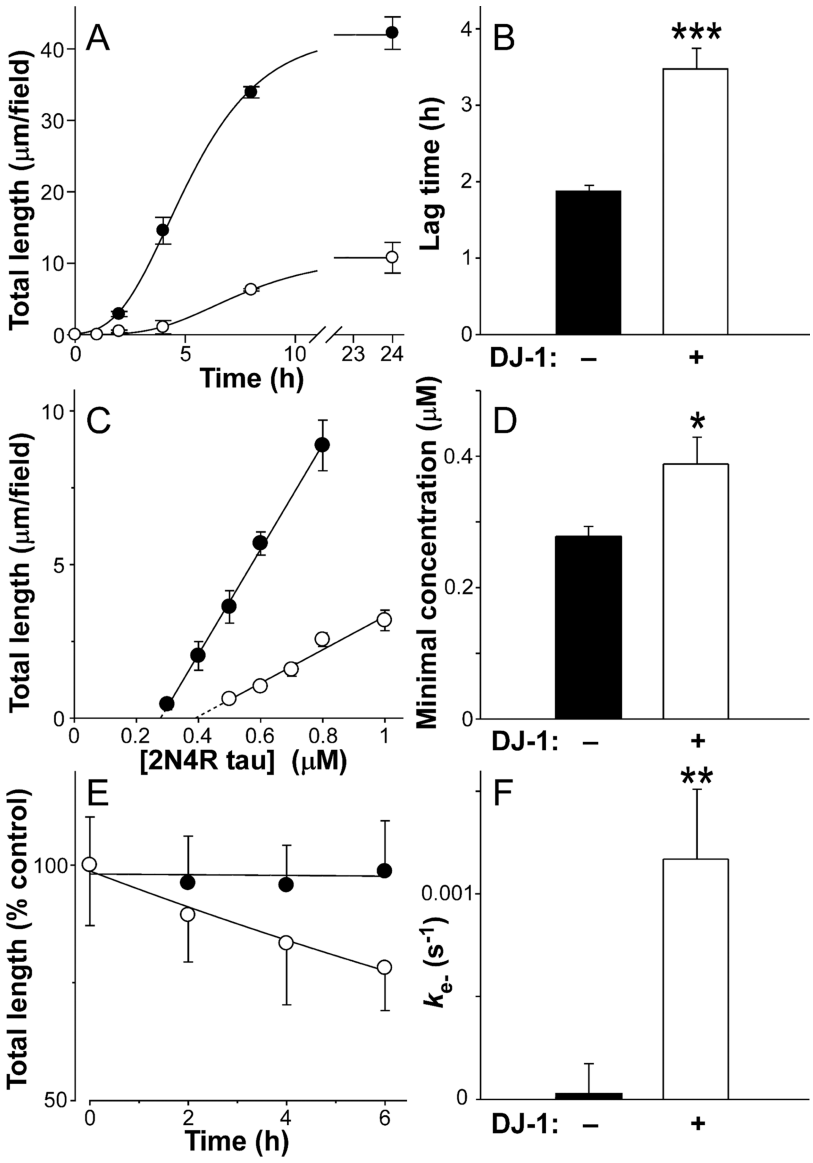

Figure 5. DJ-1 modulates tau aggregation kinetics. 2N4R tau protein was incubated under aggregation conditions (24 h at 37 °C) in the absence (solid circles) or presence (hollow circles) of purified recombinant wild-type DJ-1 (1:1 DJ-1:tau ratio) and then assayed for filament formation as a function of time using TEM. (A) Aggregation time series (1.5 μM tau, absence and presence of 1:1 DJ-1:tau), where each data point represents total filament lengths/field calculated from electron microscopy images ± S.D. (n = 4–6) and the solid lines represent the best fit of data to a three-parameter Gompertz growth function. Values for lag time were estimated from these plots. (B) Replot of lag times determined from time series, where each bar represents the lag time ± propagated SEE. The presence of stoichiometric DJ-1:tau ratios increased lag time relative to tau-only control (***p < 0.001, t-test). (C) Minimal concentration measurement in the absence and presence (1:1 DJ-1:tau ratio), where each data point represents total filament length/field at aggregation plateau as a function of bulk tau concentration (mean ± S.D. of triplicate determinations) and the solid lines represent linear regression analysis. The abscissa intercept was obtained by extrapolation (dotted lines) and taken as the minimal concentration (K_{min}). (D) Data replots, where each bar represents the K_{min} ± propagated S.E.E. The presence of DJ-1 increased K_{min} relative to tau-only control (*p < 0.05). (E) Disaggregation rate measurement. Tau filaments taken at the aggregation plateau were incubated in the presence or absence of 1:1 DJ-1:tau ratio and then assayed for total length as a function of time by TEM. Each data point represents the total filament length per field ± S.D. (n = 3), whereas the solid line represents the best fit of data points by a simple exponential decay function. The first-order decay constant k_{app} was estimated from each regression and used in conjunction with filament length and number at time t = 0 to calculate dissociation rate constant k_{e^-}. (F) Replot of data, where each bar represents estimated k_{e^-}. The addition of DJ-1 induced filament disaggregation (**p < 0.01).

required to support filament formation increased significantly in the presence of DJ-1 (Figure 5C,D). To determine whether this effect could destabilize filaments, 2N4R tau was aggregated to plateau and then incubated for an additional 6 h in the absence and presence of DJ-1. In the absence of DJ-1, total filament length was stable, reflecting minimal changes in equilibrium between tau monomers and filament ends under these conditions. In contrast, the presence of DJ-1 induced the time-dependent disaggregation of the filament population with first-order kinetics as predicted for endwise depolymerization[58,59] (Figure 5E). The dissociation rate constant (k_{e^-}) calculated from these data was 1.2 × 10^{-3} s^{-1} (Figure 5F). Together, these data reveal that stoichiometric levels of DJ-1 both slow the rate and lower the extent of tau fibrillation while shifting the equilibrium at filament ends to destabilize mature aggregates.

https://doi.org/10.1021/acs.biochem.2c00581
Biochemistry 2023, 62, 976–988

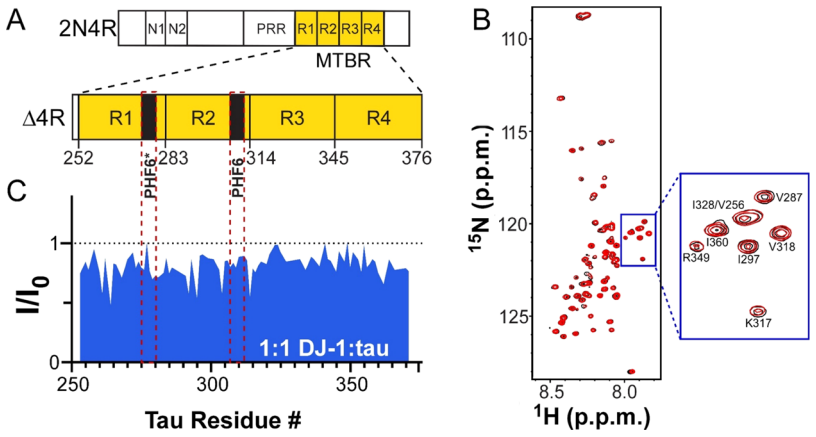

Figure 6. DJ-1 interacts with the tau microtubule-binding repeat region. (A) Schematic diagram of 2N4R tau comprising N-terminal alternatively spliced (N1 and N2), proline-rich (PRR), and microtubule-binding (MTBR) regions. The MTBR (highlighted in yellow) is composed of four imperfect repeats (R1−R4) containing two hexapeptides implicated in tau aggregate nucleation (PHF6* and PHF6). Tau truncation mutant Δ4R tau consists only of the MTBR defined on the basis of sequence alignment.[67] (B) Superposition of 2D $^{1}H-^{15}N$ HSQC spectra of Δtau (50 μM) in the absence (black) and presence (red) of equimolar concentrations of DJ-1. (C) Binding profile on Δ4R probed by NMR spectroscopy after addition of DJ-1 into $^{1}H-^{15}N$ Δ4R at 1:1 molar ratio. Changes in NMR signal intensity ratios (I/I_0) are plotted against tau residue number. The red dotted lines represent the residues associated with the PHF6* and PHF6 nucleation motifs.

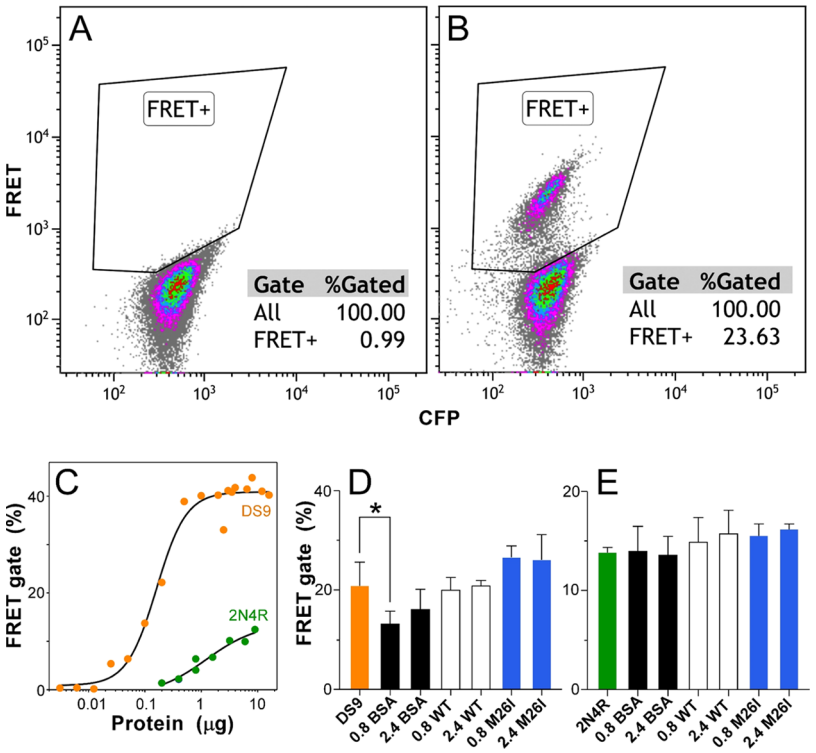

Figure 7. DJ-1 does not alter the seeding potential of tau seeds. Seeds prepared from DS9 cells and recombinant 2N4R tau protein aggregates were transfected into biosensor cells and monitored for FRET positivity using flow cytometry. Representative scatter plots in the absence (A) and presence (B) of DS9 seeds showing that the appearance of signals in the FRET-positive gate (solid lines) was seed-dependent. (C) Quantification of compensated FRET positivity rate (%) as a function of seed dose, where each point represents singlicate determination and the solid line represents best fit by a four-parameter logistic function (eq 2). EC_{50} values for DS9 and 2N4R tau seeds were 0.16 ± 0.02 and 1.2 ± 0.6 μg, respectively. (D, E) Seeding of biosensor cells by DS9 (0.16 μg) or 2N4R tau (1.2 μg) after preincubation with 0, 0.8 or 2.4 μM wild-type DJ-1 (WT), M26I mutant, or BSA control protein. Each bar represents the average (n = 3) FRET % positivity ± S.D. (*p < 0.05 compared to the seed-only condition; ANOVA with Dunnett's *post-hoc* test).

DJ-1 Interacts with the MTBR of Tau Monomer. Tau aggregation *in vivo*[60] and in recombinant systems[61,62] is mediated by its microtubule-binding region (MTBR). In 2N4R tau, this region is composed of four imperfect repeats that harbor the PHF6* and PHF6 hexapeptide motifs implicated in aggregate nucleation[63,64] (Figure 6A). Certain members of the canonical chaperome family interact with this region.[11,40] To test for direct interaction between tau and DJ-1, the MTBR of 2N4R (termed Δ4R tau) was labeled with ^{15}N, incubated in the absence and presence of DJ-1, and then subjected to two-dimensional $^{1}H-^{15}N$ heteronuclear single quantum coherence (HSQC) NMR spectroscopy. The NMR

https://doi.org/10.1021/acs.biochem.2c00581
Biochemistry 2023, 62, 976−988

approach has been used to map sites of interaction between chaperones and labeled tau proteins through the detection of changes in resonance position or intensity.[40] In the absence of DJ-1, HSQC spectra of Δ4R tau revealed a small chemical shift dispersion with amide ^{1}H frequencies clustering narrowly within the 8.6−7.6 ppm region (Figure 6B), a characteristic feature of intrinsically disordered proteins.[65] This spectrum was consistent with previous reports of 4-repeat MTBR remaining in an intrinsically disordered and monomeric state in the absence of aggregation inducers.[66] The presence of DJ-1 at stoichiometric concentration did not change the pattern (Figure 6B) but did depress signal intensity ratios throughout the MTBR, including sequences overlapping the PHF6* and PHF6 nucleation motifs (Figure 6C). These results show that DJ-1 can interact directly with tau sequences comprising the aggregation-prone MTBR when presented in an intrinsically disordered form.

DJ-1 Does Not Directly Modulate Tau Seed Activity. In addition to interacting with tau monomers, certain canonical chaperones interact with tau seeds to depress their ability to induce aggregation within naïve cell populations.[11] To investigate whether DJ-1 shared this activity, tau seeds were incubated in the presence of bovine serum albumin (BSA) control or DJ-1 and then tested for seeding activity in Tau RD P301S FRET biosensor cells.[49] Two sources of seeds were examined: products of 2N4R tau aggregation induced by Geranine G and 2N4R$^{244-372}$ proteoforms derived from HEK293 cell line DS9 (a.k.a. Clone 9[48]). The former source was used because it was composed of full-length tau, whereas the latter was included because of its ability to reproducibly seed and propagate aggregates with strain-like properties.[48] Seeding activity was detected using a flow cytometry assay[50] with compensation for overlapping emission spectra performed by a positive FRET gate constructed from seeded and nonseeded biosensor cells (Figure 7A) and validated with single-color YFP-tau and CFP-tau control cells (data not shown). As a result, seeding was quantified as the percentage of singlet/CFP^{+} cells exhibiting a positive FRET signal (Figure 7B). Both seed preparations generated concentration-dependent FRET signals when transfected into biosensor cells, with DS9 being more potent (EC_{50} = 0.16 μg lysate) and efficacious (41% cell positivity at plateau) than synthetic 2N4R conformers (EC_{50} = 1.2 μg tau; 13.8% cell positivity at plateau) (Figure 7C). However, the seeding efficiencies of DS9 (Figure 7D) and 2N4R (Figure 7E) were not altered by preincubation with either DJ-1 or M26I mutant when tested at their respective EC_{50}s. These data indicate that direct exposure of tau seeds to exogenous DJ-1 did not alter their seeding potential in this model system.

DISCUSSION

This study reveals that DJ-1 exhibits chaperone activity toward full-length 2N4R human tau protein. We find that the interaction resembles the "holdase" activity of canonical chaperones[68,69] in favoring the intrinsically disordered monomeric state of tau as a client and being ATP independent. It also is low affinity, consistent with the reported failure to detect soluble DJ-1/tau complexes by co-immunoprecipitation.[70] Although we find that the tau MTBR can mediate DJ-1/tau interaction, it cannot be excluded that sequences outside this region also contribute to the binding of full-length tau isoforms.

DJ-1 interaction with full-length tau at stoichiometric ratios extends aggregation lag time (which for nucleation-dependent aggregation varies inversely with nucleation rates)[51] and elevates minimal concentrations required to support entry into the aggregation pathway. The altered equilibrium at filament ends also destabilizes mature aggregates, leading to first-order disaggregation kinetics resembling those reported upon dilution of tau aggregates below the minimal concentration[5] or exposure to aggregation inhibitors that sequester tau monomers.[59] In these cases, first-order kinetics result from passive endwise dissociation of tau from the filament ends. In contrast, incubation of preformed tau seeds composed of full-length tau or its MTBR with DJ-1 did not modulate their seeding efficiencies. These data indicate that DJ-1 lacks the disaggregase activity displayed by certain ATP-dependent chaperones in this model system.[11] Nonetheless, prion-like seeding also requires protein monomers as substrate, and the partial sequestration of tau protein by DJ-1 is likely to depress the rate of prion-like templating similar to other monomer-dependent interactions. Overall, the holdase activity of wild-type DJ-1 dimer can protect full-length tau protein from interactions that drive aggregation.

Although not upregulated in AD as part of an adaptive response to stress like certain canonical chaperones, DJ-1 is regulated post-translationally through oxidation of Cys residues, including C106. Oxidation of C106 up to its sulfinic acid form (i.e., C106-SO_2H) has minimal effects on DJ-1 dimeric structure but enhances its ability to engage specific clients such as α-synuclein.[71] Oxidation also regulates DJ-1 subcellular distribution so that it can access binding partners localized to organelles, including stress granules[72] and mitochondria (reviewed[21]). However, further C106 oxidation to sulfonic acid form (i.e., C106-SO_3H) owing to chronic oxidative stress destabilizes dimeric DJ-1 structure and leads to irreversible inactivation.[73,74] Here, we found that oxidation incompetent C106A mutant retains full tau chaperone activity, indicating that oxidation is not required for interaction with this specific client. These data predict that DJ-1 can protect full-length tau protein against aggregation under basal conditions in the absence of oxidative stress.

DJ-1 functions normally as a soluble homodimer, but a fraction of it also forms supramolecular proteoforms that have been reported as "inclusions" when observed within cells or brain tissue and "high-molecular-weight" (HMW) complexes when detected biochemically.[70,75] Most HMW complexes range from 200 to 500 kDa[75,76] (although even larger species have been reported)[70] and consist of both homotypic and heterotypic species. HMW complex formation can be induced by the presence of clients such as α-synuclein,[77] by osmotic or oxidative stress,[72,78] by phosphate ion,[79] or, in the case of bacterial homologue Hsp31, by zinc cation.[80] Here, we found that large complexes detectable by TEM, laser light scattering spectroscopy, and sedimentation also could be induced by incubation of DJ-1 in the presence of tau protein under near-physiological buffer conditions and bulk tau concentrations. These data suggest a potential source of the insoluble tau/DJ-1 complexes observed in tauopathic neurodegenerative disease tissue, including AD and frontotemporal dementias.[26,27]

Although heterotypic HMW complexes have been proposed to represent functional assemblies for certain constituent proteins,[76] their sequestration of DJ-1 reportedly renders them nonfunctional with respect to chaperone activity.[75] Disease-causing DJ-1 mutants can raise complex-forming propensity

https://doi.org/10.1021/acs.biochem.2c00581
Biochemistry 2023, 62, 976−988

still further resulting in DJ-1 inactivation. For example, M26I maintains dimeric structure in solution, but exhibits decreased secondary structure and thermodynamic stability,[24] which in turn fosters aggregation and loss of function.[23,81] The surface missense mutant E64D also greatly increases aggregation propensity, as evidenced by inclusion formation in HEK293 cells.[77] Here, we found that both M26I and E64D have significantly lower tau chaperone activity than wild-type DJ-1. These data show that two distinct classes of disease-associated DJ-1 mutants modulate tau chaperone activity in parallel with previous observations.

To date, only one homozygous *PARK7* mutant linked to familial PD (case 22 years of age) has been characterized pathologically, revealing a phenotype resembling advanced-stage sporadic PD with respect to α-synuclein-bearing Lewy bodies but to only early-stage AD with respect to tau-bearing neurofibrillary pathology.[29] If DJ-1 functions toward chaperone tau misfolding and aggregation in parallel with α-synuclein and other clients, why does a core DJ-1 mutant generate primarily Lewy body pathology over tauopathy? One possible contributing factor is that tau protein normally associates with the microtubule cytoskeleton rather than with DJ-1 in cytosol. Release of tau from its high-affinity physiological binding partner into cytosol and accumulation above the minimal concentration required for aggregation require tau hyperphosphorylation.[82,83] The stresses that cause tau to incorporate up to 6−9 mol/mol phosphate[84,85] are not fully understood, but the process is age-dependent, with the onset of sporadic AD typically being over 65 years of age[86] and of frontotemporal lobar degeneration tauopathy over 50 years of age.[87] In contrast, early-onset PD, including cases caused by *PARK7* mutants, appears between ages 20 and 40.[88] Under conditions of early-onset disease, release of tau into cytosol may be the rate-limiting step for aggregation rather than loss of DJ-1 chaperone activity. Indeed, complete knockout of DJ-1 in mice reproduces neither the synucleinopathy nor neurodegeneration of PD,[89,90] indicating that DJ-1 is not the governing modulator of lesion formation under these experimental conditions. Further work will be required to identify disease stages when DJ-1-mediated effects on tau and α-synuclein aggregation become rate-determining.

CONCLUSIONS

In summary, these data provide biochemical evidence that DJ-1 molecular chaperone activity depresses tau aggregation propensity and that its effectiveness is weakened by mutations linked to familial disease. The findings suggest an opportunity to control tau as well as α-synuclein aggregation and toxicity in tauopathies through stabilizing or enhancing DJ-1 activity. Such approaches are needed because comorbid cases may not respond to therapies that target a single pathology. Understanding the mechanisms that contribute to comorbidity could be important for providing a new approach to treating neurodegenerative diseases.

ASSOCIATED CONTENT

Accession Codes

2N4R tau: UniProtKB P10636-8 and DJ-1: UniProtKB Q99497.

AUTHOR INFORMATION

Corresponding Author

Jeff Kuret − *Department of Biological Chemistry and Pharmacology, The Ohio State University College of Medicine, Columbus, Ohio 43210, United States;* orcid.org/0000-0002-8083-8406; Email: kuret.3@osu.edu

Authors

Daniela Jimenez-Harrison − *Medical Scientist Training Program, The Ohio State University, Columbus, Ohio 43210, United States;* orcid.org/0000-0003-0786-7988

Carol J. Huseby − *Department of Biological Chemistry and Pharmacology, The Ohio State University College of Medicine, Columbus, Ohio 43210, United States*

Claire N. Hoffman − *Department of Biological Chemistry and Pharmacology, The Ohio State University College of Medicine, Columbus, Ohio 43210, United States*

Steven Sher − *Medical Scientist Training Program, The Ohio State University, Columbus, Ohio 43210, United States*

Dalton Snyder − *Department of Chemistry and Biochemistry, The Ohio State University College of Medicine, Columbus, Ohio 43210, United States*

Brayden Seal − *Department of Biological Chemistry and Pharmacology, The Ohio State University College of Medicine, Columbus, Ohio 43210, United States*

Chunhua Yuan − *Campus Chemical Instrument Center, The Ohio State University College of Medicine, Columbus, Ohio 43210, United States*

Hongjun Fu − *Department of Neuroscience, The Ohio State University College of Medicine, Columbus, Ohio 43210, United States*

Vicki Wysocki − *Department of Chemistry and Biochemistry, The Ohio State University College of Medicine, Columbus, Ohio 43210, United States*

Flaviano Giorgini − *Department of Genetics and Genome Biology, University of Leicester, Leicester LE1 7RH, United Kingdom*

Complete contact information is available at: https://pubs.acs.org/10.1021/acs.biochem.2c00581

Funding

This project was supported by a grant from the National Institutes of Health (RF1AG054018 [to J.K.]). Mass spectrometry experiments were supported by the Resource for Native Mass Spectrometry Guided Structural Biology (P41GM128577 [to V.W.]). C.N.H. was supported by Molecular Biophysics Training grant T32 GM118291.

Notes

The authors declare no competing financial interest.

ACKNOWLEDGMENTS

The authors thank Dr. Marc Diamond, University of Texas Southwestern, for providing DS9 and single-color cell control HEK293 cell lines and Dr. Rosa Lapalombella and the Experimental Hematology Laboratory at The Ohio State University Comprehensive Cancer Center (OSUCCC) for the usage of the BD LSR Fortessa. The authors acknowledge resources from the Campus Microscopy and Imaging Facility (CMIF) and the OSUCCC Microscopy Shared Resource (MSR), the Ohio State University.

■ ABBREVIATIONS

AD, Alzheimer's disease; BCA, bicinchoninic acid; IMAC, immobilized metal affinity chromatography; MTBR, microtubule-binding region; nMS, native mass spectroscopy; PD, Parkinson's disease; TEM, transmission electron microscopy; TEV, Tobacco Etch Virus

■ REFERENCES

(1) Limorenko, G.; Lashuel, H. A. Revisiting the grammar of Tau aggregation and pathology formation: how new insights from brain pathology are shaping how we study and target Tauopathies. *Chem. Soc. Rev.* **2022**, *51*, 513−565.

(2) Gendron, T. F.; Petrucelli, L. The role of tau in neurodegeneration. *Mol. Neurodegener.* **2009**, *4*, 13.

(3) Tracy, T. E.; Gan, L. Tau-mediated synaptic and neuronal dysfunction in neurodegenerative disease. *Curr. Opin. Neurobiol.* **2018**, *51*, 134−138.

(4) Friedhoff, P.; von Bergen, M.; Mandelkow, E. M.; Davies, P.; Mandelkow, E. A nucleated assembly mechanism of Alzheimer paired helical filaments. *Proc. Natl. Acad. Sci. U.S.A.* **1998**, *95*, 15712−15717.

(5) Congdon, E. E.; Kim, S.; Bonchak, J.; Songrug, T.; Matzavinos, A.; Kuret, J. Nucleation-dependent tau filament formation: the importance of dimerization and an estimation of elementary rate constants. *J. Biol. Chem.* **2008**, *283*, 13806−13816.

(6) Ramachandran, G.; Udgaonkar, J. B. Understanding the kinetic roles of the inducer heparin and of rod-like protofibrils during amyloid fibril formation by Tau protein. *J. Biol. Chem.* **2011**, *286*, 38948−38959.

(7) Vaquer-Alicea, J.; Diamond, M. I. Propagation of Protein Aggregation in Neurodegenerative Diseases. *Annu. Rev. Biochem.* **2019**, *88*, 785−810.

(8) Mocanu, M. M.; Nissen, A.; Eckermann, K.; Khlistunova, I.; Biernat, J.; Drexler, D.; Petrova, O.; Schonig, K.; Bujard, H.; Mandelkow, E.; Zhou, L.; Rune, G.; Mandelkow, E. M. The potential for β-structure in the repeat domain of tau protein determines aggregation, synaptic decay, neuronal loss, and coassembly with endogenous Tau in inducible mouse models of tauopathy. *J. Neurosci.* **2008**, *28*, 737−748.

(9) Hartl, F. U.; Bracher, A.; Hayer-Hartl, M. Molecular chaperones in protein folding and proteostasis. *Nature* **2011**, *475*, 324−332.

(10) Brehme, M.; Voisine, C.; Rolland, T.; Wachi, S.; Soper, J. H.; Zhu, Y.; Orton, K.; Villella, A.; Garza, D.; Vidal, M.; Ge, H.; Morimoto, R. I. A chaperome subnetwork safeguards proteostasis in aging and neurodegenerative disease. *Cell Rep.* **2014**, *9*, 1135−1150.

(11) Mok, S. A.; Condello, C.; Freilich, R.; Gillies, A.; Arhar, T.; Oroz, J.; Kadavath, H.; Julien, O.; Assimon, V. A.; Rauch, J. N.; Dunyak, B. M.; Lee, J.; Tsai, F. T. F.; Wilson, M. R.; Zweckstetter, M.; Dickey, C. A.; Gestwicki, J. E. Mapping interactions with the chaperone network reveals factors that protect against tau aggregation. *Nat. Struct. Mol. Biol.* **2018**, *25*, 384−393.

(12) Lucas, J. I.; Marin, I. A new evolutionary paradigm for the Parkinson disease gene DJ-1. *Mol. Biol. Evol.* **2006**, *24*, 551−561.

(13) Bandyopadhyay, S.; Cookson, M. R. Evolutionary and functional relationships within the DJ1 superfamily. *BMC Evol. Biol.* **2004**, *4*, 6.

(14) Lee, S. J.; Kim, S. J.; Kim, I. K.; Ko, J.; Jeong, C. S.; Kim, G. H.; Park, C.; Kang, S. O.; Suh, P. G.; Lee, H. S.; Cha, S. S. Crystal structures of human DJ-1 and Escherichia coli Hsp31, which share an evolutionarily conserved domain. *J. Biol. Chem.* **2003**, *278*, 44552−44559.

(15) Shendelman, S.; Jonason, A.; Martinat, C.; Leete, T.; Abeliovich, A. DJ-1 is a redox-dependent molecular chaperone that inhibits alpha-synuclein aggregate formation. *PLoS Biol.* **2004**, *2*, No. e362.

(16) Sajjad, M. U.; Green, E. W.; Miller-Fleming, L.; Hands, S.; Herrera, F.; Campesan, S.; Khoshnan, A.; Outeiro, T. F.; Giorgini, F.; Wyttenbach, A. DJ-1 modulates aggregation and pathogenesis in models of Huntington's disease. *Hum. Mol. Genet.* **2014**, *23*, 755−766.

(17) Zondler, L.; Miller-Fleming, L.; Repici, M.; Goncalves, S.; Tenreiro, S.; Rosado-Ramos, R.; Betzer, C.; Straatman, K. R.; Jensen, P. H.; Giorgini, F.; Outeiro, T. F. DJ-1 interactions with alpha-synuclein attenuate aggregation and cellular toxicity in models of Parkinson's disease. *Cell Death Dis.* **2014**, *5*, No. e1350.

(18) Wilson, M. A.; Collins, J. L.; Hod, Y.; Ringe, D.; Petsko, G. A. The 1.1-A resolution crystal structure of DJ-1, the protein mutated in autosomal recessive early onset Parkinson's disease. *Proc. Natl. Acad. Sci. U.S.A.* **2003**, *100*, 9256−9261.

(19) Andreeva, A.; Bekkhozhin, Z.; Omertassova, N.; Baizhumanov, T.; Yeltay, G.; Akhmetali, M.; Toibazar, D.; Utepbergenov, D. The apparent deglycase activity of DJ-1 results from the conversion of free methylglyoxal present in fast equilibrium with hemithioacetals and hemiaminals. *J. Biol. Chem.* **2019**, *294*, 18863−18872.

(20) Mazza, M. C.; Shuck, S. C.; Lin, J.; Moxley, M. A.; Termini, J.; Cookson, M. R.; Wilson, M. A. DJ-1 is not a deglycase and makes a modest contribution to cellular defense against methylglyoxal damage in neurons. *J. Neurochem.* **2022**, *162*, 245−261.

(21) Wilson, M. A. The role of cysteine oxidation in DJ-1 function and dysfunction. *Antioxid. Redox Signal.* **2011**, *15*, 111−122.

(22) Repici, M.; Giorgini, F. DJ-1 in Parkinson's Disease: Clinical Insights and Therapeutic Perspectives. *J. Clin. Med.* **2019**, *8*, 1377.

(23) Lakshminarasimhan, M.; Maldonado, M. T.; Zhou, W.; Fink, A. L.; Wilson, M. A. Structural impact of three Parkinsonism-associated missense mutations on human DJ-1. *Biochemistry* **2008**, *47*, 1381−1392.

(24) Malgieri, G.; Eliezer, D. Structural effects of Parkinson's disease linked DJ-1 mutations. *Protein Sci.* **2008**, *17*, 855−868.

(25) Kumaran, R.; Kingsbury, A.; Coulter, I.; Lashley, T.; Williams, D.; de Silva, R.; Mann, D.; Revesz, T.; Lees, A.; Bandopadhyay, R. DJ-1 (PARK7) is associated with 3R and 4R tau neuronal and glial inclusions in neurodegenerative disorders. *Neurobiol. Dis.* **2007**, *28*, 122−132.

(26) Rizzu, P.; Hinkle, D. A.; Zhukareva, V.; Bonifati, V.; Severijnen, L. A.; Martinez, D.; Ravid, R.; Kamphorst, W.; Eberwine, J. H.; Lee, V. M.; Trojanowski, J. Q.; Heutink, P. DJ-1 colocalizes with tau inclusions: a link between parkinsonism and dementia. *Ann. Neurol.* **2004**, *55*, 113−118.

(27) Neumann, M.; Muller, V.; Gorner, K.; Kretzschmar, H. A.; Haass, C.; Kahle, P. J. Pathological properties of the Parkinson's disease-associated protein DJ-1 in alpha-synucleinopathies and tauopathies: relevance for multiple system atrophy and Pick's disease. *Acta Neuropathol.* **2004**, *107*, 489−496.

(28) Choi, J.; Sullards, M. C.; Olzmann, J. A.; Rees, H. D.; Weintraub, S. T.; Bostwick, D. E.; Gearing, M.; Levey, A. I.; Chin, L. S.; Li, L. Oxidative damage of DJ-1 is linked to sporadic Parkinson and Alzheimer diseases. *J. Biol. Chem.* **2006**, *281*, 10816−10824.

(29) Taipa, R.; Pereira, C.; Reis, I.; Alonso, I.; Bastos-Lima, A.; Melo-Pires, M.; Magalhaes, M. DJ-1 linked parkinsonism (PARK7) is associated with Lewy body pathology. *Brain* **2016**, *139*, 1680−1687.

(30) Robinson, J. L.; Lee, E. B.; Xie, S. X.; Rennert, L.; Suh, E.; Bredenberg, C.; Caswell, C.; Van Deerlin, V. M.; Yan, N.; Yousef, A.; Hurtig, H. I.; Siderowf, A.; Grossman, M.; McMillan, C. T.; Miller, B.; Duda, J. E.; Irwin, D. J.; Wolk, D.; Elman, L.; McCluskey, L.; Chen-Plotkin, A.; Weintraub, D.; Arnold, S. E.; Brettschneider, J.; Lee, V. M.; Trojanowski, J. Q. Neurodegenerative disease concomitant proteinopathies are prevalent, age-related and APOE4-associated. *Brain* **2018**, *141*, 2181−2193.

(31) Zhang, X.; Gao, F.; Wang, D.; Li, C.; Fu, Y.; He, W.; Zhang, J. Tau Pathology in Parkinson's Disease. *Front. Neurol.* **2018**, *9*, 809.

(32) Giasson, B. I.; Forman, M. S.; Higuchi, M.; Golbe, L. I.; Graves, C. L.; Kotzbauer, P. T.; Trojanowski, J. Q.; Lee, V. M. Initiation and synergistic fibrillization of tau and α-synuclein. *Science* **2003**, *300*, 636−640.

(33) Spina, S.; La Joie, R.; Petersen, C.; Nolan, A. L.; Cuevas, D.; Cosme, C.; Hepker, M.; Hwang, J. H.; Miller, Z. A.; Huang, E. J.; Karydas, A. M.; Grant, H.; Boxer, A. L.; Gorno-Tempini, M. L.; Rosen, H. J.; Kramer, J. H.; Miller, B. L.; Seeley, W. W.; Rabinovici, G.

D.; Grinberg, L. T. Comorbid neuropathological diagnoses in early versus late-onset Alzheimer's disease. *Brain* **2021**, *144*, 2186−2198.
(34) Beach, T. G.; Malek-Ahmadi, M. Alzheimer's Disease Neuropathological Comorbidities are Common in the Younger-Old. *J. Alzheimers Dis.* **2021**, *79*, 389−400.
(35) Schafer, K. N.; Cisek, K.; Huseby, C. J.; Chang, E.; Kuret, J. Structural determinants of Tau aggregation inhibitor potency. *J. Biol. Chem.* **2013**, *288*, 32599−32611.
(36) Raran-Kurussi, S.; Cherry, S.; Zhang, D.; Waugh, D. S. Removal of Affinity Tags with TEV Protease. *Methods Mol. Biol.* **2017**, *1586*, 221−230.
(37) Walker, J. M. The Bicinchoninic Acid (BCA) Assay for Protein Quantitation. In *The Protein Protocols Handbook*; Walker, J. M., Ed.; Humana Press: Totowa, NJ, 1996; pp 11−14.
(38) Marley, J.; Lu, M.; Bracken, C. A method for efficient isotopic labeling of recombinant proteins. *J. Biomol. NMR* **2001**, *20*, 71−75.
(39) Barré, P.; Eliezer, D. Structural transitions in tau k18 on micelle binding suggest a hierarchy in the efficacy of individual microtubule-binding repeats in filament nucleation. *Protein Sci.* **2013**, *22*, 1037−1048.
(40) Karagöz, G.; Duarte, A. M.; Akoury, E.; Ippel, H.; Biernat, J.; Moran Luengo, T.; Radli, M.; Didenko, T.; Nordhues, B. A.; Veprintsev, D. B.; Dickey, C. A.; Mandelkow, E.; Zweckstetter, M.; Boelens, R.; Madl, T.; Rudiger, S. G. Hsp90-Tau complex reveals molecular basis for specificity in chaperone action. *Cell* **2014**, *156*, 963−974.
(41) VanAernum, Z. L.; Gilbert, J. D.; Belov, M. E.; Makarov, A. A.; Horning, S. R.; Wysocki, V. H. Surface-Induced Dissociation of Noncovalent Protein Complexes in an Extended Mass Range Orbitrap Mass Spectrometer. *Anal. Chem.* **2019**, *91*, 3611−3618.
(42) Marty, M. T.; Baldwin, A. J.; Marklund, E. G.; Hochberg, G. K.; Benesch, J. L.; Robinson, C. V. Bayesian deconvolution of mass and ion mobility spectra: from binary interactions to polydisperse ensembles. *Anal. Chem.* **2015**, *87*, 4370−4376.
(43) Huseby, C. J.; Kuret, J. Analyzing Tau Aggregation with Electron Microscopy. *Methods Mol. Biol.* **2016**, *1345*, 101−112.
(44) Chirita, C. N.; Necula, M.; Kuret, J. Anionic micelles and vesicles induce tau fibrillization in vitro. *J. Biol. Chem.* **2003**, *278*, 25644−25650.
(45) Schneider, C. A.; Rasband, W. S.; Eliceiri, K. W. NIH Image to ImageJ: 25 years of image analysis. *Nat. Methods* **2012**, *9*, 671−675.
(46) Rasband, W. S. *ImageJ*, National Institutes of Health, 2022.
(47) Necula, M.; Kuret, J. A static laser light scattering assay for surfactant-induced tau fibrillization. *Anal. Biochem.* **2004**, *333*, 205−215.
(48) Sanders, D. W.; Kaufman, S. K.; DeVos, S. L.; Sharma, A. M.; Mirbaha, H.; Li, A.; Barker, S. J.; Foley, A. C.; Thorpe, J. R.; Serpell, L. C.; Miller, T. M.; Grinberg, L. T.; Seeley, W. W.; Diamond, M. I. Distinct tau prion strains propagate in cells and mice and define different tauopathies. *Neuron* **2014**, *82*, 1271−1288.
(49) Holmes, B. B.; Furman, J. L.; Mahan, T. E.; Yamasaki, T. R.; Mirbaha, H.; Eades, W. C.; Belaygorod, L.; Cairns, N. J.; Holtzman, D. M.; Diamond, M. I. Proteopathic tau seeding predicts tauopathy in vivo. *Proc. Natl. Acad. Sci. U.S.A.* **2014**, *111*, E4376−4385.
(50) Furman, J. L.; Diamond, M. I. FRET and Flow Cytometry Assays to Measure Proteopathic Seeding Activity in Biological Samples. *Methods Mol. Biol.* **2017**, *1523*, 349−359.
(51) Evans, K. C.; Berger, E. P.; Cho, C. G.; Weisgraber, K. H.; Lansbury, P. T., Jr. Apolipoprotein E is a kinetic but not a thermodynamic inhibitor of amyloid formation: implications for the pathogenesis and treatment of Alzheimer disease. *Proc. Natl. Acad. Sci. U.S.A.* **1995**, *92*, 763−767.
(52) Necula, M.; Kuret, J. Electron microscopy as a quantitative method for investigating tau fibrillization. *Anal. Biochem.* **2004**, *329*, 238−246.
(53) Kanaan, N. M.; Grabinski, T. Neuronal and Glial Distribution of Tau Protein in the Adult Rat and Monkey. *Front. Mol. Neurosci.* **2021**, *14*, No. 607303.
(54) Zhong, Q.; Congdon, E. E.; Nagaraja, H. N.; Kuret, J. Tau isoform composition influences rate and extent of filament formation. *J. Biol. Chem.* **2012**, *287*, 20711−20719.
(55) Chirita, C. N.; Congdon, E. E.; Yin, H.; Kuret, J. Triggers of full-length tau aggregation: a role for partially folded intermediates. *Biochemistry* **2005**, *44*, 5862−5872.
(56) Copeland, R. A. *Evaluation of Enzyme Inhibitors In Drug Discovery*, 2nd ed.; Wiley: Hoboken, NJ, 2013; p 538.
(57) Arhar, T.; Shkedi, A.; Nadel, C. M.; Gestwicki, J. E. The interactions of molecular chaperones with client proteins: why are they so weak? *J. Biol. Chem.* **2021**, *297*, No. 101282.
(58) Kristofferson, D.; Karr, T. L.; Purich, D. L. Dynamics of linear protein polymer disassembly. *J. Biol. Chem.* **1980**, *255*, 8567−8572.
(59) Necula, M.; Kuret, J. Site-specific pseudophosphorylation modulates the rate of tau filament dissociation. *FEBS Lett.* **2005**, *579*, 1453−1457.
(60) Zhang, W.; Tarutani, A.; Newell, K. L.; Murzin, A. G.; Matsubara, T.; Falcon, B.; Vidal, R.; Garringer, H. J.; Shi, Y.; Ikeuchi, T.; Murayama, S.; Ghetti, B.; Hasegawa, M.; Goedert, M.; Scheres, S. H. W. Novel tau filament fold in corticobasal degeneration. *Nature* **2020**, *580*, 283−287.
(61) Zhang, W.; Falcon, B.; Murzin, A. G.; Fan, J.; Crowther, R. A.; Goedert, M.; Scheres, S. H. Heparin-induced tau filaments are polymorphic and differ from those in Alzheimer's and Pick's diseases. *eLife* **2019**, *8*, No. e43584.
(62) Dregni, A. J.; Mandala, V. S.; Wu, H.; Elkins, M. R.; Wang, H. K.; Hung, I.; DeGrado, W. F.; Hong, M. In vitro 0N4R tau fibrils contain a monomorphic beta-sheet core enclosed by dynamically heterogeneous fuzzy coat segments. *Proc. Natl. Acad. Sci. U.S.A.* **2019**, *116*, 16357−16366.
(63) von Bergen, M.; Friedhoff, P.; Biernat, J.; Heberle, J.; Mandelkow, E. M.; Mandelkow, E. Assembly of tau protein into Alzheimer paired helical filaments depends on a local sequence motif (^{306}VQIVYK^{311}) forming β structure. *Proc. Natl. Acad. Sci. U.S.A.* **2000**, *97*, 5129−5134.
(64) Li, W.; Lee, V. M. Characterization of two VQIXXK motifs for tau fibrillization in vitro. *Biochemistry* **2006**, *45*, 15692−15701.
(65) Gibbs, E. B.; Cook, E. C.; Showalter, S. A. Application of NMR to studies of intrinsically disordered proteins. *Arch. Biochem. Biophys.* **2017**, *628*, 57−70.
(66) Kaur, J.; Giri, A.; Bhattacharya, M. The protein-surfactant stoichiometry governs the conformational switching and amyloid nucleation kinetics of tau K18. *Eur. Biophys. J.* **2020**, *49*, 425−434.
(67) Goedert, M.; Spillantini, M. G.; Potier, M. C.; Ulrich, J.; Crowther, R. A. Cloning and sequencing of the cDNA encoding an isoform of microtubule-associated protein tau containing four tandem repeats: differential expression of tau protein mRNAs in human brain. *EMBO J.* **1989**, *8*, 393−399.
(68) Mitra, R.; Wu, K.; Lee, C.; Bardwell, J. C. A. ATP-Independent Chaperones. *Annu. Rev. Biophys.* **2022**, *51*, 409−429.
(69) Hall, D. On the nature of the optimal form of the holdase-type chaperone stress response. *FEBS Lett.* **2020**, *594*, 43−66.
(70) Meulener, M. C.; Graves, C. L.; Sampathu, D. M.; Armstrong-Gold, C. E.; Bonini, N. M.; Giasson, B. I. DJ-1 is present in a large molecular complex in human brain tissue and interacts with alpha-synuclein. *J. Neurochem.* **2005**, *93*, 1524−1532.
(71) Zhou, W.; Zhu, M.; Wilson, M. A.; Petsko, G. A.; Fink, A. L. The oxidation state of DJ-1 regulates its chaperone activity toward alpha-synuclein. *J. Mol. Biol.* **2006**, *356*, 1036−1048.
(72) Repici, M.; Hassanjani, M.; Maddison, D. C.; Garcao, P.; Cimini, S.; Patel, B.; Szego, E. M.; Straatman, K. R.; Lilley, K. S.; Borsello, T.; Outeiro, T. F.; Panman, L.; Giorgini, F. The Parkinson's Disease-Linked Protein DJ-1 Associates with Cytoplasmic mRNP Granules During Stress and Neurodegeneration. *Mol. Neurobiol.* **2019**, *56*, 61−77.
(73) Kiss, R.; Zhu, M.; Jojart, B.; Czajlik, A.; Solti, K.; Forizs, B.; Nagy, E.; Zsila, F.; Beke-Somfai, T.; Toth, G. Structural features of human DJ-1 in distinct Cys106 oxidative states and their relevance to

its loss of function in disease. *Biochim. Biophys. Acta* **2017**, *1861*, 2619−2629.
(74) Catazaro, J.; Andrews, T.; Milkovic, N. M.; Lin, J.; Lowe, A. J.; Wilson, M. A.; Powers, R. (15)N CEST data and traditional model-free analysis capture fast internal dynamics of DJ-1. *Anal. Biochem.* **2018**, *542*, 24−28.
(75) Baulac, S.; LaVoie, M. J.; Strahle, J.; Schlossmacher, M. G.; Xia, W. Dimerization of Parkinson's disease-causing DJ-1 and formation of high molecular weight complexes in human brain. *Mol. Cell. Neurosci.* **2004**, *27*, 236−246.
(76) Piston, D.; Alvarez-Erviti, L.; Bansal, V.; Gargano, D.; Yao, Z.; Szabadkai, G.; Odell, M.; Puno, M. R.; Bjorkblom, B.; Maple-Grodem, J.; Breuer, P.; Kaut, O.; Larsen, J. P.; Bonn, S.; Moller, S. G.; Wullner, U.; Schapira, A. H. V.; Gegg, M. E. DJ-1 is a redox sensitive adapter protein for high molecular weight complexes involved in regulation of catecholamine homeostasis. *Hum. Mol. Genet.* **2017**, *26*, 4028−4041.
(77) Repici, M.; Straatman, K. R.; Balduccio, N.; Enguita, F. J.; Outeiro, T. F.; Giorgini, F. Parkinson's disease-associated mutations in DJ-1 modulate its dimerization in living cells. *J. Mol. Med.* **2013**, *91*, 599−611.
(78) Solti, K.; Kuan, W. L.; Forizs, B.; Kustos, G.; Mihaly, J.; Varga, Z.; Herberth, B.; Moravcsik, E.; Kiss, R.; Karpati, M.; Mikes, A.; Zhao, Y.; Imre, T.; Rochet, J. C.; Aigbirhio, F.; Williams-Gray, C. H.; Barker, R. A.; Toth, G. DJ-1 can form beta-sheet structured aggregates that co-localize with pathological amyloid deposits. *Neurobiol. Dis.* **2020**, *134*, No. 104629.
(79) Cha, S. S.; Jung, H. I.; Jeon, H.; An, Y. J.; Kim, I. K.; Yun, S.; Ahn, H. J.; Chung, K. C.; Lee, S. H.; Suh, P. G.; Kang, S. O. Crystal structure of filamentous aggregates of human DJ-1 formed in an inorganic phosphate-dependent manner. *J. Biol. Chem.* **2008**, *283*, 34069−34075.
(80) Kim, J.; Choi, D.; Cha, S. Y.; Oh, Y. M.; Hwang, E.; Park, C.; Ryu, K. S. Zinc-mediated Reversible Multimerization of Hsp31 Enhances the Activity of Holding Chaperone. *J. Mol. Biol.* **2018**, *430*, 1760−1772.
(81) Hulleman, J. D.; Mirzaei, H.; Guigard, E.; Taylor, K. L.; Ray, S. S.; Kay, C. M.; Regnier, F. E.; Rochet, J. C. Destabilization of DJ-1 by familial substitution and oxidative modifications: implications for Parkinson's disease. *Biochemistry* **2007**, *46*, 5776−5789.
(82) Biernat, J.; Mandelkow, E. M.; Schroter, C.; Lichtenberg-Kraag, B.; Steiner, B.; Berling, B.; Meyer, H.; Mercken, M.; Vandermeeren, A.; Goedert, M.; et al. The switch of tau protein to an Alzheimer-like state includes the phosphorylation of two serine-proline motifs upstream of the microtubule binding region. *EMBO J.* **1992**, *11*, 1593−1597.
(83) Bramblett, G. T.; Trojanowski, J. Q.; Lee, V. M. Regions with abundant neurofibrillary pathology in human brain exhibit a selective reduction in levels of binding-competent tau and accumulation of abnormal tau-isoforms (A68 proteins). *Lab. Invest.* **1992**, *66*, 212−222.
(84) Köpke, E.; Tung, Y. C.; Shaikh, S.; Alonso, A. C.; Iqbal, K.; Grundke-Iqbal, I. Microtubule-associated protein tau. Abnormal phosphorylation of a non-paired helical filament pool in Alzheimer disease. *J. Biol. Chem.* **1993**, *268*, 24374−24384.
(85) Ksiezak-Reding, H.; Liu, W. K.; Yen, S. H. Phosphate analysis and dephosphorylation of modified tau associated with paired helical filaments. *Brain Res.* **1992**, *597*, 209−219.
(86) Scheltens, P.; De Strooper, B.; Kivipelto, M.; Holstege, H.; Chetelat, G.; Teunissen, C. E.; Cummings, J.; van der Flier, W. M. Alzheimer's disease. *Lancet* **2021**, *397*, 1577−1590.
(87) Erkkinen, M. G.; Kim, M. O.; Geschwind, M. D. Clinical Neurology and Epidemiology of the Major Neurodegenerative Diseases. *Cold Spring Harb. Perspect. Biol.* **2018**, *10*, No. a033118.
(88) Quinn, N.; Critchley, P.; Marsden, C. D. Young onset Parkinson's disease. *Mov. Disord.* **1987**, *2*, 73−91.
(89) Goldberg, M. S.; Pisani, A.; Haburcak, M.; Vortherms, T. A.; Kitada, T.; Costa, C.; Tong, Y.; Martella, G.; Tscherter, A.; Martins, A.; Bernardi, G.; Roth, B. L.; Pothos, E. N.; Calabresi, P.; Shen, J. Nigrostriatal dopaminergic deficits and hypokinesia caused by inactivation of the familial Parkinsonism-linked gene DJ-1. *Neuron* **2005**, *45*, 489−496.
(90) Chen, L.; Cagniard, B.; Mathews, T.; Jones, S.; Koh, H. C.; Ding, Y.; Carvey, P. M.; Ling, Z.; Kang, U. J.; Zhuang, X. Age-dependent motor deficits and dopaminergic dysfunction in DJ-1 null mice. *J. Biol. Chem.* **2005**, *280*, 21418−21426.

https://doi.org/10.1021/acs.biochem.2c00581
Biochemistry 2023, 62, 976−988